https://doi.org/10.5194/egusphere-2024-589
Preprint. Discussion started: 15 March 2024

First evaluation of the GEMS glyoxal products against TROPOMI and ground-based measurements

Eunjo S. Ha[1], Rokjin J. Park[1], Hyeong-Ahn Kwon[2], Gitaek T. Lee[1], Sieun D. Lee[1], Seunga Shin[1], Dong-Won Lee[3], Hyunkee Hong[3], Christophe Lerot[4*], Isabelle De Smedt[4], Francois Hendrick[4], and Hitoshi Irie[5]

[1]School of Earth and Environmental Science, Seoul National University, Seoul, Republic of Korea
[2]Department of Environmental & Energy Engineering, The University of Suwon, Suwon, Republic of Korea
[3]National Institute of Environmental Research, Incheon, Republic of Korea
[4]Royal Belgian Institute for Space Aeronomy (BIRA-IASB), Brussels, Belgium
[5]Department of Earth Sciences, Chiba University, Chiba, Japan
*Now at Constellr, Brussels, Belgium

Correspondence to: Rokjin J. Park (rjpark@snu.ac.kr) and Hyeong-Ahn Kwon (hakwon@suwon.ac.kr)

Abstract. The Geostationary Environment Monitoring Spectrometer (GEMS) aboard the GEO-KOMPSAT-2B satellite is the first geostationary satellite launched to monitor the environment. GEMS conducts hourly measurements during the day over East and Southeast Asia. This work presents glyoxal (CHOCHO) vertical column densities (VCDs) retrieved from GEMS, with optimal settings for glyoxal retrieval based on sensitivity tests involving reference spectrum sampling and fitting window selection. We evaluated GEMS glyoxal VCDs by comparing them to TROPOMI and MAX-DOAS ground-based observations. On average, GEMS and TROPOMI VCDs show a spatial correlation coefficient of 0.63, increasing to 0.87 for Northeast Asia. While GEMS and TROPOMI demonstrate similar monthly variations in the Indochinese peninsula regions ($R > 0.67$), variations differ in other areas. Specifically, GEMS VCDs are lower in the summer and higher in the winter than TROPOMI VCDs in Northeast Asia, potentially due to a polluted reference spectrum and high NO_2 concentrations. This trend also occurs in comparing monthly variations between GEMS and MAX-DOAS VCDs. When averaged hourly, GEMS and MAX-DOAS VCDs exhibit similar diurnal variations, especially at stations in Japan (Chiba, Kasuga, and Fukue).

1 Introduction

Glyoxal (CHOCHO) is the smallest di-carbonyl compound with a short atmospheric lifetime of fewer than 3 hours during daylight hours (Volkamer et al., 2006). Some glyoxal is directly emitted through biomass burning and biofuel utilization; however, the majority is produced via the oxidation of non-methane volatile organic compounds (NMVOCs) (Fu et al., 2008). Glyoxal is predominantly removed from the atmosphere by photolysis and reaction with OH radicals (Volkamer et al., 2005). When glyoxal oxidizes in the presence of nitrogen oxides, it contributes to the secondary formation

https://doi.org/10.5194/egusphere-2024-589
Preprint. Discussion started: 15 March 2024

of ozone. Furthermore, the high solubility of glyoxal facilitates its absorption by aqueous aerosols and cloud droplets, forming secondary organic aerosols (SOAs) (Fu et al., 2008; Lerot et al., 2021). Given that ozone and SOAs are harmful air pollutants and agents of climate change, comprehending their VOC precursors is critical for managing air quality and climate.

The number of VOCs detectable from space is limited compared to the numerous VOCs existing in the atmosphere. Glyoxal and formaldehyde (HCHO) are examples of non-methane volatile organic compounds (NMVOCs) that are retrieved using ultraviolet (UV) to visible wavelength. These compounds, predominantly produced by the oxidation of other VOCs and characterized by short atmospheric lifetimes, provide valuable insights into local VOC emissions when measured. Satellite observations offer a comprehensive overview for estimating top-down emissions due to their extensive spatial coverage compared to ground-based, in situ measurements (Choi et al., 2022). The different yields of formaldehyde and glyoxal from NMVOCs add additional information to constrain individual NMVOC emissions. For example, formaldehyde is typically produced in large amounts from alkenes, while glyoxal is a high-yield product of aromatic compounds (Dufour et al., 2009; Cao et al., 2018; Chan Miller et al., 2016). Chan Miller et al. (2017) noted that while formaldehyde and glyoxal data are closely linked, the precise measurements of glyoxal could provide additional information, especially in environments with low nitrogen oxides (NOx). Furthermore, due to the shorter atmospheric lifetime of glyoxal compared to formaldehyde, elevated concentrations of glyoxal are indicative of the immediate vicinity of wildfires and areas with intense photochemical reactions (Vrekoussis et al., 2010; Alvarado et al., 2020). The ratio of glyoxal to formaldehyde (RGF = [CHOCHO]/[HCHO]) has been used in several studies to differentiate the origins of VOC emissions, distinguishing between anthropogenic or biogenic sources (Vrekoussis et al., 2010; Digangi et al., 2012).

The observation of glyoxal from a sun-synchronous satellite was conducted by the SCanning Imaging Absorption spectroMeter for Atmospheric CHartographY (SCIAMACHY) instrument, which was launched in 2002 (Wittrock et al., 2006). This instrument has a pixel size of 60 km along the track and 120 km across the track, enabling global coverage in six days. Building upon SCIAMACHY's achievements, glyoxal columns with improved spatial and temporal resolutions have been retrieved from the Global Ozone Monitoring Experiment-2 (GOME-2) (Lerot et al., 2010; Vrekoussis et al., 2009) and Ozone Monitoring Instrument (OMI) (Chan Miller et al., 2014; Alvarado et al., 2014). The spatial resolutions for GOME-2 and OMI glyoxal data are 80 × 40 km² and 13 × 24 km², respectively, offering global coverage in 1.5 days and one day. Glyoxal columns retrieved from the TROPOspheric Monitoring Instrument (TROPOMI) exhibit the highest spatial resolution, at 3.5 × 5.5 km², with an overpass of 13:30 local time (Lerot et al., 2021). These Low Earth Orbit (LEO) satellite instruments have significantly contributed to mapping the spatial distribution of glyoxal globally. However, they are limited in their ability to capture the diurnal variations of glyoxal, which are crucial for understanding its emissions, transport, and chemical reactions.

To address the limitations of sun-synchronous satellites, the Geostationary Environment Monitoring Spectrometer (GEMS) was launched aboard the GEO-KOMPSAT-2B satellite in February 2020 (Kim et al., 2020), providing trace gas and aerosol measurements as the first geostationary satellite. GEMS performs hourly measurements across East and

https://doi.org/10.5194/egusphere-2024-589
Preprint. Discussion started: 15 March 2024

Southeast Asia, including parts of India, ranging from 6–10 times a day depending on the season. This study presents the retrieval of glyoxal data from GEMS using an algorithm that Kwon et al. (2019) developed for formaldehyde retrieval. The adaptation of this algorithm for glyoxal retrieval is detailed in Sect. 2. We evaluate the GEMS glyoxal product by comparing it with TROPOMI data in Sect. 3, and GEMS glyoxal products are validated against ground-based observations in Sect. 4.

2 Description of the GEMS glyoxal algorithm

For glyoxal retrievals, we use the same retrieval algorithm for formaldehyde for GEMS, and detailed descriptions of the algorithm are explained in Kwon et al. (2019) and Lee et al. (2023 Preprint). Here, we only focus on the distinctive features of glyoxal retrievals. The GEMS system attributes and parameters for radiance fitting are summarized in Table 1. Retrieving GEMS glyoxal vertical column densities (VCDs) involves three steps. First, a radiative transfer equation is fitted to back-scattered radiances within a glyoxal's spectral absorption range. This spectral fitting process yields a glyoxal slant column density (SCD), representing the integrated concentration along the mean photon path. Subsequently, the SCD is converted to the VCD by dividing the air mass factor (AMF). AMF converts SCD to VCD by accounting for the light path varying with viewing geometry, the atmospheric scattering from clouds, and the vertical profile of glyoxal. Lastly, background correction is performed by adding simulated concentration over the reference sector.

Glyoxal is a weak absorber within the absorption range of glyoxal compared to ozone and nitrogen dioxide, and the amount of glyoxal in the atmosphere is relatively small. Therefore, strong absorbers and instrument noise can significantly constrain glyoxal retrievals. We use co-added products with 16 (4×4) GEMS pixels to enhance the signal-to-noise ratio for GEMS glyoxal retrievals, including radiance, irradiance, surface reflectance, and cloud products. This approach reduces a spatial resolution of ~14 × 32 km² for glyoxal over Seoul, South Korea, but results in the stable spectral fitting to obtain glyoxal SCDs.

2.1 Spectral fitting

The spectral fitting yields glyoxal SCDs by fitting the modeled radiative transfer equation to measured radiances, as described in Eq. (6) by Kwon et al. (2019). The modeled radiative transfer equation demonstrates the attenuation of the reference spectrum by gas absorptions based on the Lambert-Beer law. Solar irradiance is commonly used as the reference spectrum in the UV to visible wavelengths. However, using solar irradiance to retrieve weak absorbers could result in systematic biases caused by spectral interference or instrumental limitations (Lerot et al., 2021). Therefore, we use measured radiances as the reference spectrum in the spectral fitting. We obtain the reference spectrum by averaging radiances from clean pixels for the past three days for each track and scene in the reference sector (120–150° E).

The spectral fitting accounts for absorption by chemical species, including CHOCHO, NO_2, O_3, O_4, H_2O (liquid), and H_2O (vapor). In addition, the GEMS instrument's polarization sensitivity is included as a pseudo-absorber since GEMS

https://doi.org/10.5194/egusphere-2024-589
Preprint. Discussion started: 15 March 2024

is not equipped with a polarization scrambler. The polarization sensitivity values measured before the launch of the GEMS are depicted in Figure 5 of Lee et al. (2023 Preprint). The polarization sensitivity values at the fitting window of glyoxal are incorporated for the spectral fitting. We use the most updated absorption cross-sections available as of now. NO_2 absorption cross-sections at two temperatures (220, 294 K) are used, considering the strong influence of NO_2 at the glyoxal absorption range (Table 1). Glyoxal retrieval is highly sensitive to the selection of the fitting window due to its low optical depth in the atmosphere (Alvarado et al., 2014). We tested fitting windows that included glyoxal's absorption wavelength and selected an optimal fitting window of 433.0–461.5 nm. This fitting window generally showed low fitting RMS and column uncertainty over the domain, low column amounts in oceans and deserts, and higher column amounts where glyoxal sources exist.

Figures 1a and 1b show glyoxal SCDs and root-mean-square values of spectral fitting residuals (fitting RMS) retrieved using radiance references. The 1st and 99th percentiles and an average of fitting RMS in August 2020 are 3.6×10^{-4}, 8.0×10^{-4}, and 5.6×10^{-4}, respectively. The fitting RMS are large over the Tibetan plateau and the southwestern part of the domain despite low VCDs, indicating the low credibility of the retrieval. Figure 1c shows one case of fitted optical depth and fitting residuals in Indonesia (15 August 2020; 0.6° N, 123.9° E). The fitting residuals oscillate centered along the optical depth, indicating that fitting residuals have no specific features.

Table 1. Summary of operational GEMS system attributes and parameters for radiance fitting.

GEMS system attributes	Spectral range	300 – 500 nm
	Spectral resolution	< 0.6 nm
	Wavelength sampling	< 0.2 nm
	Field of regard (FOR)	≥ 5000 (N/S) km × 5000 (E/W) km (5° S–45° N, 75–145° E)
	Spatial resolution (at Seoul)	< for glyoxal (4 × 4 co-added pixels)
	Duty cycle	6 ~ 10 times per day (six times in winter, ten times in summer)
	Imaging time	≤ 30 min
Radiance fitting parameters	Fitting window (calibration window)	433.0–461.5 nm (431.3–463.5 nm)
	Reference	Three days average of measured radiances from easternmost swaths (120–150° E) under clear-sky condition (cloud fraction < 0.4)
	Solar reference spectrum	Chance and Kurucz (2010)
	Absorption cross-sections	CHOCHO at 296 K (Volkamer et al., 2005)

https://doi.org/10.5194/egusphere-2024-589
Preprint. Discussion started: 15 March 2024

		O_3 at 223 K (Serdyuchenko et al., 2014) NO_2 at 220 K and 294 K (Vandaele et al., 1998) O_4 at 293 K (Finkenzeller and Volkamer, 2022) H_2O (vapor) at 283 K (Gordon et al., 2022) H_2O (liquid) at 296 K (Mason et al., 2016)
	Ring effect	Chance and Kurucz (2010)
	Common mode	Online common mode from easternmost swaths (120–150° E) for a day
	Polarization correction	Polarization sensitivity vector at the central pixel of charge-coupled-device (CCD)
	Scaling and baseline polynomials	Third order

2.2 Air mass factor

In the presence of atmospheric scattering, AMF can be formulated in terms of scattering weight (w_z), and vertical shape factor (S_z) (Palmer et al., 2001).

$$AMF = \int_0^\infty w_z S_z dz \quad (1)$$

Scattering weight is a function of the solar zenith angle, viewing zenith angle, relative azimuth angle, surface reflectance, cloud pressure, and cloud fraction. We use different values of these parameters for each latitude, longitude, and month. A look-up table of the scattering weight at 448 nm is constructed using VLIDORT v2.6 (Spurr, 2006). Surface reflectance is obtained from OMI Lambertian Equivalent Reflectance (LER) Climatology products (Kleipool, 2010), and cloud pressure and fraction are obtained from GEMS L2 cloud products.

The vertical shape factor is calculated using a global 3-D chemical transport model (GEOS-Chem v13.0.0) with 47 vertical layers and 0.25°×0.3125° horizontal resolutions in Asia (Bey et al., 2001; Wang et al., 2004). The KORUS v5 inventory was used for anthropogenic emissions (Woo, n.d.). Biogenic emissions are taken from MEGANv2.1 (Guenther et al., 2012), and biomass burning emissions are taken from the monthly GFED4 inventory (van der Werf et al., 2010). We use monthly mean hourly vertical profiles from August 2020 to July 2021 to better represent diurnal variations.

https://doi.org/10.5194/egusphere-2024-589
Preprint. Discussion started: 15 March 2024

2.3 Background correction

Glyoxal SCDs retrieved from the spectral fitting using the radiance reference are differential slant column densities (dSCDs) that do not include background columns over the clean reference sector (120–150° E). Therefore, we use simulated vertical columns in the reference sector for background correction, as shown in Eq. (2).

$$VCD(i,j) = \frac{SCD(i,j)}{AMF(i,j)} = \frac{dSCD(i,j)+AMF_0(lat)VCD_m(lat)}{AMF(i,j)} \quad (2)$$

VCD_m is simulated monthly mean hourly VCD zonally averaged in the reference sector (120–150° E) from the model used to construct AMF. Figure 2 shows glyoxal VCDs with and without background correction. The difference is large in the high latitudes where the reference sector is close to polluted sources. However, the background contribution shown in Figure 2c is lower than the offset value (10^{14} molecules cm^{-2}) used for the background correction of the TROPOMI (Lerot et al., 2021) and SCIAMACHY (Wittrock, 2006) glyoxal column. The offset value of 10^{14} molecules cm^{-2} is selected from the ship-based measurement over the Pacific Ocean (Sinreich et al., 2010). As the background contribution for GEMS glyoxal VCD is low, the VCDs with (Figure 2a) and without background correction (Figure 2b) do not represent significant differences. The low value of VCD_m is due to the underestimation of glyoxal columns from the current chemical transport models (CTM) (Li et al., 2018; Silva et al., 2018). Previous studies suggested that the emissions of precursor VOCs are underestimated (Kwon et al., 2021; Choi et al., 2022) and that the oxidative chemistry producing glyoxal is not well represented (Silva et al., 2018).

2.4 Random uncertainties and observation noise

Random uncertainties in slant columns (σ_s) are fitting uncertainties mainly resulting from instrument noise and can be calculated using Eq. (3) (Kwon et al., 2019).

$$\sigma_{s,j}^2 = RMS^2 \frac{m}{m-n} C_{j,j} C_{j,j} \quad (3)$$

RMS is the root-mean-square value of fitting residuals, m, and n are the number of spectral grids and fitting parameters, $C_{j,j}$ is diagonal components of a covariance matrix, and j is the subscript for fitting parameters. The 1st to the 99th percentiles of random uncertainties are 3.6×10^{14} and 1.6×10^{15} molecules cm^{-2} in August 2020, with a mean of 8.6×10^{14} molecules cm^{-2}. The random uncertainties of GEMS are higher than TROPOMI, as the 1st to the 99th percentiles of TROPOMI random uncertainties are 4.4×10^{14} and 1.0×10^{15} molecules cm^{-2} in August 2020 with a mean of 6.5×10^{14} molecules cm^{-2} in the GEMS field of regards (FOR).

The observation noise is large compared to the actual signal for glyoxal retrieval, and the credibility of glyoxal retrieval is known to be low in oceans due to low concentration and interference with liquid water absorption (Alvarado et al., 2014). Figure 3 illustrates VCDs over the Pacific Ocean and the observation noise estimated from its standard deviation. We followed the analysis from Lerot et al. (2021) to estimate the noise level of GEMS VCDs and compared them with TROPOMI VCDs. While Lerot et al. (2021) analyzed VCDs over 180–120° W, we analyzed GEMS VCDs over 130–146° E

https://doi.org/10.5194/egusphere-2024-589
Preprint. Discussion started: 15 March 2024

due to the limited coverage of the geostationary satellite. We filter out pixels over land with cloud cover (cloud fraction > 0.4) for the analysis. VCDs binned in 5° latitude bands range from 0.9×10^{14} to 2.1×10^{14} molecules cm^{-2}, which is notably lower than the scatter for all data. GEMS glyoxal observation noise ranges from 3.7×10^{14} to 7.0×10^{14} molecules cm^{-2}, comparable to the noise of TROPOMI VCDs.

3 Comparison with TROPOMI data

We evaluate GEMS glyoxal retrieval by comparing GEMS glyoxal VCDs with TROPOMI from August 2020 to July 2021. For comparing GEMS and TROPOMI products, GEMS VCDs are averaged in 0.5□x 0.5□grids weighted by the overlapping area between pixels and grid boxes. For comparison, we used hourly GEMS data (FinalAlgorithmFlags = 0, cloud fraction < 0.4) at the TROPOMI overpass time in each region. TROPOMI L3 glyoxal data with a spatial resolution of 0.05° x 0.05°□are regridded into the same 0.5° x 0.5°□grids for the comparison.

Figures 5a and 5b show GEMS and TROPOMI glyoxal VCDs averaged from August 2020 to July 2021 at 11:30–15:30 local time. We find good consistencies between the two products over the whole domain, with a correlation coefficient of 0.63 and a regression slope 1.26 (Figure 5d). Both products show high VCDs in the Indochinese Peninsula and populated cities such as Shanghai and Guangdong due to biogenic or anthropogenic emissions of VOCs. However, GEMS is slightly higher than TROPOMI in Northeast Asia. This discrepancy may be partly due to the elevated NO_2 concentration. Lerot et al. (2021) conducted an empirical correction for strong NO_2 absorption for TROPOMI, which decreased glyoxal concentrations as a function of NO_2 SCDs. The correction of GEMS glyoxal VCDs accounting for the strong absorption NO_2 needs to be developed as the current operational product (GEMS glyoxal V2.0) does not consider this effect.

In the west of the domain, the negative bias of GEMS VCDs compared to TROPOMI occurs due to the GEMS's high viewing zenith angle (Figure 5c). A similar negative bias is also found in formaldehyde retrieval (Lee et al., 2023 Preprint). GEMS glyoxal VCDs are even negative in parts of the Indian Ocean, the area outside the dashed green line depicted in Figure 4, in which no clear reasons for this issue have been found yet. Excluding this region in our scatter increases the correlation coefficient to 0.71 between the two products (Figure 5e). We also find an excellent agreement (R=0.87) between the two products in Northeast Asia, defined as Domain 2 in Figure 4, which includes Eastern China and Korea (Figure 5f).

Figure 6 shows monthly mean VCDs of GEMS and TROPOMI averaged in six regions (Figure 4) from August 2020 to December 2022. Values are high in Cambodia and Myanmar, especially in spring, due to biomass burning influences, which are consistently captured by the two products with relatively high correlation coefficients (0.67–0.89). However, GEMS is somewhat inconsistent in regions located in Northeast Asia, such as Korea, North China Plain (NCP), and Yangtze River Delta (YRD), showing low correlation coefficients (0.16–0.40) with TROPOMI, mainly driven by too high GEMS values in winter. Positive bias of GEMS in winter may be due to high NO_2 concentration, which is notable in NCP. Mean

https://doi.org/10.5194/egusphere-2024-589
Preprint. Discussion started: 15 March 2024

GEMS NO_2 SCDs over NCP are 1.57×10^{16} molecules cm^{-2} in June 2021 and 2.74×10^{16} molecules cm^{-2} in December 2021. The relative differences of GEMS and TROPOMI ($\frac{GEMS-TROPOMI}{TROPOMI}$) glyoxal VCDs in NCP are -5% and 167% in June 2021 and December 2021, respectively. If we empirically correct glyoxal SCDs using the same linear regression equation derived from the TROPOMI glyoxal retrieval algorithm ($-8.75 \times 10^{12} - 7.01 \times 10^{-3} \times NO_2\ SCD$; Lerot et al., 2021), the relative differences are -33% and 23% in June and December 2021, respectively. While the negative bias in the summer worsens, the positive bias in the winter improves significantly.

The underestimation of GEMS VCDs compared to TROPOMI in the summer in Northeast Asia could be attributed to the polluted reference spectrum. Most of the scan area from August to September 2020 was a nominal daily or full central scan (Figure 1 of Kwon et al., 2019). However, since October 2020, the scan area has changed to a full central or full western scan, decreasing the area for sampling radiance reference. Although the simulated VCDs are averaged in the same area for the background correction, this does not fully compensate for the reduction in the differential slant column since GEOS-Chem underestimates glyoxal concentration (Bates and Jacob, 2019; Silva et al., 2018; Chan Miller et al., 2017). This could result in the low seasonal variation of GEMS VCDs, especially in the high latitudes, where the reference sector is somewhat polluted.

Figure 7 demonstrates the sensitivity of retrieved glyoxal VCDs to the selection of reference spectrum depending on the scan schedules. During the in-orbit test period (IOT), observations were frequently taken as a nominal daily scan, which covers 90–150° E, enabling us to obtain the reference spectrum over 120–150° E. Figure 7a illustrates glyoxal VCDs retrieved with the reference spectrum taken from the reference sector of 120–150° E in August 2020. Figure 7b shows the same retrieved glyoxal VCDs but with the reference spectrum averaged over 120–133° E, which is the narrow reference sector limited by the full western scan, frequently conducted after the IOT. Values in Figure 7b are about 22% lower than those in Figure 7a, possibly due to the effect of local pollution on the reference spectrum. The largest discrepancy occurs in 28–40° N, including Korea, NCP, and YRD (Figure 7c). Obtaining the reference spectrum from the clean region is very crucial for the GEMS glyoxal product.

4 Comparison with MAX-DOAS observations

This section evaluates GEMS VCDs with ground-based Multi-Axis Differential Optical Absorption Spectroscopy (MAX-DOAS) observations (Lerot et al., 2021) at Chiba, Kasuga, Fukue, Phimai, Pantnagar, Haldwani, Seoul, and Xianghe (Figure 4) from August 2020 to December 2021. MAX-DOAS data at Xianghe are operated by BIRA-IASB (Hendrick et al., 2014), and data for the other six stations are operated by CERES (Irie et al., 2011). Each institution uses different fitting intervals and profile retrieval algorithms. The data from Pantnagar and Haldwani were merged and shown in the same subplot, considering their geographical proximity and the lack of temporal overlap; measurements in Pantnagar were made until January 2021, and those in Haldwani were from June 2021. We filtered out MAX-DOAS observations with random

https://doi.org/10.5194/egusphere-2024-589
Preprint. Discussion started: 15 March 2024

uncertainty higher than 30%, primarily from the Pantnagar site. We averaged GEMS VCD pixels within 0.72° from the MAX-DOAS stations for comparison, considering the spatial resolution of GEMS glyoxal data. All the data are hourly and coherently sampled at the same local time.

Figure 8 compares monthly mean GEMS and MAX-DOAS glyoxal VCDs. Both show a reasonable agreement in Northeast Asia (Chiba, Kasuga, Fukue, Seoul, and Xianghe) despite some discrepancies of GEMS being low in summer and high in winter, as shown in the comparison with TROPOMI. In Phimai, GEMS VCDs are slightly lower than MAX-DOAS VCDs but show similar seasonal variations. At the Pantnagar and Haldwani sites, uncertainties are high due to the few MAX-DOAS observations and possible aerosol contamination (Lerot et al., 2021). Underestimation of GEMS VCDs in India is also found in the formaldehyde product, which could be attributed to the longer light path at high viewing zenith angles (Lee et al., 2023 Preprint).

Figure 9 compares hourly mean GEMS and MAX-DOAS glyoxal VCDs. We find a good agreement between the two datasets regarding glyoxal diurnal variations in Japan (Chiba, Kasuga, and Fukue). Chiba is located near Tokyo and shows elevated concentrations compared to rural sites like Kasuga and Fukue. GEMS underestimates VCDs at the Phimai, Pantnagar, and Haldwani sites, located west of other sites. In Seoul, GEMS and MAX-DOAS VCDs are similar until 14:00 local time and diverge afterward. The continuous increase in the MAS-DOAS observations is not reasonable though further validation is necessary. GEMS and MAX-DOAS VCDs at Xianghe are consistent except at low solar zenith angles, as fewer samples are available.

5 Conclusion and discussions

This study presents the inaugural retrieval of glyoxal columns from the geostationary satellite. To reduce the uncertainty associated with SCD retrieval, we selected optimal settings for the spectral fitting based on sensitivity tests involving reference spectrum and fitting window. The retrieved SCDs are converted to VCDs using AMF derived from high-resolution GEOS-Chem simulations. The background correction is the final process to add column amounts over the reference sector. The capability of GEMS to observe hourly glyoxal VCDs offers unparalleled temporal resolution, enriching our understanding of VOC emissions and transport.

We compared the retrieved glyoxal VCDs with other satellite and ground-based measurements. GEMS and TROPOMI VCDs generally show similar spatial distribution; however, GEMS VCDs tend to be higher in the north-eastern domain and lower in the south-western domain than TROPOMI VCDs. While monthly variations of GEMS VCDs correlate well with those of TROPOMI and MAX-DOAS VCDs in the Indochinese peninsula regions, variations differ in Northeast Asia. The biases of GEMS may result from the interference with high NO_2 concentration, polluted reference spectrum, and high viewing zenith angle.

https://doi.org/10.5194/egusphere-2024-589
Preprint. Discussion started: 15 March 2024

To address the overestimation in the high NO_2 regions, the wavelength dependency of NO_2 absorption must be considered. Correction of the glyoxal column with NO_2 concentration could improve the consistency of GEMS VCDs with other measurements regarding spatial distribution and temporal variation. This is because the overestimation becomes more pronounced in winter when NO_2 concentration is higher. However, subtracting the glyoxal column as a function of NO_2 concentration could exacerbate the underestimation of GEMS glyoxal VCDs in summer in Northeast Asia. Therefore, simultaneous work must be performed to resolve the polluted reference spectrum issue. We could consider methods such as filtering pixels representing high glyoxal concentrations simulated from the CTM over the reference sector or utilizing synthetic radiances from the RTM.

The limited field of regard of GEMS poses significant challenges in finding a clean reference sector. While background concentrations in the reference sector are corrected from the simulated concentrations, this is insufficient to resolve bias in GEMS VCDs because the CTM used for background correction underestimates glyoxal VCDs. Enhancing the fidelity of CTMs, particularly in terms of emission and oxidative chemistry of precursor VOCs, is required to mitigate bias in GEMS VCDs across monthly and diurnal variations. While the availability of in-situ glyoxal measurements for reference purposes is limited, the Airborne and Satellite Investigation of Asian Air Quality (ASIA-AQ) campaign presents a promising opportunity. This initiative will comprehensively evaluate observed and simulated glyoxal columns and enhance our understanding of atmospheric processes at scales finer than those resolvable by satellite pixels.

https://doi.org/10.5194/egusphere-2024-589
Preprint. Discussion started: 15 March 2024

Data availability.

The GEMS Level 1C data are available on request from the National Institute of Environmental Research (NIER) – Environmental Satellite Center (ESC). The GEMS Level 2 products are available at https://nesc.nier.go.kr/ko/html/index.do (last access: 28 February 2024). Access to TROPOMI glyoxal tropospheric column data is possible via the GLYRETRO website at https://glyretro.aeronomie.be/index.php/data-menu-item/request-data-test/new-data (last access: 28 February 2024) (Lerot et al., 2021).

Author contributions.

ESH, RJP, and HAK designed the study, carried out the analyses, and wrote the manuscript. GTL, SDL, and SS participated in the algorithm development. DWL and HH supported the GEMS instrument. CL and IDS provided the TROPOMI glyoxal product. FH, HI carried out the MAX-DOAS measurement.

Competing interests.

The contact author has declared that none of the authors has any competing interests.

Special issue statement.

This article is part of the special issue "GEMS: first year in operation (AMT/ACP inter-journal SI)". It is not associated with a conference.

Acknowledgements.

The authors thank the GEMS science team and the Environment Satellite Center (ESC) of National Institute of Environmental Research (NIER) for supporting the GEMS glyoxal retrieval algorithm development.

Financial support.

This research was supported by a grant from the Nation Institute of Environmental Research (NIER), funded by the Korea Ministry of Environment (MOE) of the Republic of Korea (NIER-2023-04-02-050).

References

Alvarado, L. M. A., Richter, A., Vrekoussis, M., Wittrock, F., Hilboll, A., Schreier, S. F., and Burrows, J. P.: An improved glyoxal retrieval from OMI measurements, Atmos Meas Tech, 7, 4133–4150, https://doi.org/10.5194/amt-7-4133-2014, 2014.

https://doi.org/10.5194/egusphere-2024-589
Preprint. Discussion started: 15 March 2024

Alvarado, L. M. A., Richter, A., Vrekoussis, M., Hilboll, A., Kalisz Hedegaard, A. B., Schneising, O., and Burrows, J. P.: Unexpected long-range transport of glyoxal and formaldehyde observed from the Copernicus Sentinel-5 Precursor satellite during the 2018 Canadian wildfires, Atmos Chem Phys, 20, 2057–2072, https://doi.org/10.5194/acp-20-2057-2020, 2020.

Bates, K. H. and Jacob, D. J.: A new model mechanism for atmospheric oxidation of isoprene: Global effects on oxidants, nitrogen oxides, organic products, and secondary organic aerosol, Atmos Chem Phys, 19, 9613–9640, https://doi.org/10.5194/acp-19-9613-2019, 2019.

Bey, I., Jacob, D. J., Yantosca, R. M., Logan, J. A., Field, B. D., Fiore, A. M., Li, Q., Liu, H. Y., Mickley, L. J., and Schultz, M. G.: Global modeling of tropospheric chemistry with assimilated meteorology: Model description and evaluation, Journal of Geophysical Research Atmospheres, 106, 23073–23095, https://doi.org/10.1029/2001JD000807, 2001.

Cao, H., Fu, T. M., Zhang, L., Henze, D. K., Miller, C. C., Lerot, C., Abad, G. G., De Smedt, I., Zhang, Q., Van Roozendael, M., Hendrick, F., Chance, K., Li, J., Zheng, J., and Zhao, Y.: Adjoint inversion of Chinese non-methane volatile organic compound emissions using space-based observations of formaldehyde and glyoxal, Atmos Chem Phys, 18, 15017–15046, https://doi.org/10.5194/acp-18-15017-2018, 2018.

Chan Miller, C., Gonzalez Abad, G., Wang, H., Liu, X., Kurosu, T., Jacob, D. J., and Chance, K.: Glyoxal retrieval from the ozone monitoring instrument, Atmos Meas Tech, 7, 3891–3907, https://doi.org/10.5194/amt-7-3891-2014, 2014.

Chan Miller, C., J Jacob, D., González Abad, G., and Chance, K.: Hotspot of glyoxal over the Pearl River delta seen from the OMI satellite instrument: Implications for emissions of aromatic hydrocarbons, Atmos Chem Phys, 16, 4631–4639, https://doi.org/10.5194/acp-16-4631-2016, 2016.

Chan Miller, C., Jacob, D. J., Marais, E. A., Yu, K., Travis, K. R., Kim, P. S., Fisher, J. A., Zhu, L., Wolfe, G. M., Hanisco, T. F., Keutsch, F. N., Kaiser, J., Min, K. E., Brown, S. S., Washenfelder, R. A., González Abad, G., and Chance, K.: Glyoxal yield from isoprene oxidation and relation to formaldehyde: Chemical mechanism, constraints from SENEX aircraft observations, and interpretation of OMI satellite data, Atmos Chem Phys, 17, 8725–8738, https://doi.org/10.5194/acp-17-8725-2017, 2017.

Chance, K. and Kurucz, R. L.: An improved high-resolution solar reference spectrum for earth's atmosphere measurements in the ultraviolet, visible, and near infrared, J Quant Spectrosc Radiat Transf, 111, 1289–1295, 2010.

Choi, J., Henze, D. K., Cao, H., Nowlan, C. R., González Abad, G., Kwon, H. A., Lee, H. M., Oak, Y. J., Park, R. J., Bates, K. H., Maasakkers, J. D., Wisthaler, A., and Weinheimer, A. J.: An Inversion Framework for Optimizing Non-Methane VOC Emissions Using Remote Sensing and Airborne Observations in Northeast Asia During the KORUS-AQ Field Campaign, Journal of Geophysical Research: Atmospheres, 127, https://doi.org/10.1029/2021JD035844, 2022.

Digangi, J. P., Henry, S. B., Kammrath, A., Boyle, E. S., Kaser, L., Schnitzhofer, R., Graus, M., Turnipseed, A., Weber, R. J., Hornbrook, R. S., Cantrell, C. A., Maudlin, R. L., Kim, S., Nakashima, Y., Wolfe, G. M., Kajii, Y., Apel, E. C., Goldstein, A. H., Guenther, A., Karl, T., Hansel, A., and Keutsch, F. N.: Observations of glyoxal and formaldehyde as metrics for the

https://doi.org/10.5194/egusphere-2024-589
Preprint. Discussion started: 15 March 2024

anthropogenic impact on rural photochemistry, Atmos Chem Phys, 12, 9529–9543, https://doi.org/10.5194/acp-12-9529-2012, 2012.

Dufour, G., Wittrock, F., Camredon, M., Beekmann, M., Richter, A., Aumont, B., and Burrows, J. P.: Atmospheric Chemistry and Physics SCIAMACHY formaldehyde observations: constraint for isoprene emission estimates over Europe?, Atmos. Chem. Phys, 1647–1664 pp., 2009.

Finkenzeller, H. and Volkamer, R.: O2–2 CIA in the gas phase: Cross-section of weak bands, and continuum absorption between 297–500 nm, J Quant Spectrosc Radiat Transf, 108063, 2022.

Fu, T. M., Jacob, D. J., Wittrock, F., Burrows, J. P., Vrekoussis, M., and Henze, D. K.: Global budgets of atmospheric glyoxal and methylglyoxal, and implications for formation of secondary organic aerosols, Journal of Geophysical Research Atmospheres, 113, https://doi.org/10.1029/2007JD009505, 2008.

Gordon, I. E., Rothman, L. S., Hargreaves, R. J., Hashemi, R., Karlovets, E. V., Skinner, F. M., Conway, E. K., Hill, C., Kochanov, R. V., Tan, Y., Wcisło, P., Finenko, A. A., Nelson, K., Bernath, P. F., Birk, M., Boudon, V., Campargue, A., Chance, K. V., Coustenis, A., Drouin, B. J., Flaud, J. M., Gamache, R. R., Hodges, J. T., Jacquemart, D., Mlawer, E. J., Nikitin, A. V., Perevalov, V. I., Rotger, M., Tennyson, J., Toon, G. C., Tran, H., Tyuterev, V. G., Adkins, E. M., Baker, A., Barbe, A., Canè, E., Császár, A. G., Dudaryonok, A., Egorov, O., Fleisher, A. J., Fleurbaey, H., Foltynowicz, A., Furtenbacher, T., Harrison, J. J., Hartmann, J. M., Horneman, V. M., Huang, X., Karman, T., Karns, J., Kassi, S., Kleiner, I., Kofman, V., Kwabia-Tchana, F., Lavrentieva, N. N., Lee, T. J., Long, D. A., Lukashevskaya, A. A., Lyulin, O. M., Makhnev, V. Y., Matt, W., Massie, S. T., Melosso, M., Mikhailenko, S. N., Mondelain, D., Müller, H. S. P., Naumenko, O. V., Perrin, A., Polyansky, O. L., Raddaoui, E., Raston, P. L., Reed, Z. D., Rey, M., Richard, C., Tóbiás, R., Sadiek, I., Schwenke, D. W., Starikova, E., Sung, K., Tamassia, F., Tashkun, S. A., Vander Auwera, J., Vasilenko, I. A., Vigasin, A. A., Villanueva, G. L., Vispoel, B., Wagner, G., Yachmenev, A., and Yurchenko, S. N.: The HITRAN2020 molecular spectroscopic database, J Quant Spectrosc Radiat Transf, 277, https://doi.org/10.1016/j.jqsrt.2021.107949, 2022.

Guenther, A. B., Jiang, X., Heald, C. L., Sakulyanontvittaya, T., Duhl, T., Emmons, L. K., and Wang, X.: The model of emissions of gases and aerosols from nature version 2.1 (MEGAN2.1): An extended and updated framework for modeling biogenic emissions, Geosci Model Dev, 5, 1471–1492, https://doi.org/10.5194/gmd-5-1471-2012, 2012.

Hendrick, F., Clémer, K., Wang, P., De Mazière, M., Fayt, C., Gielen, C., Hermans, C., Ma, J. Z., Pinardi, G., Stavrakou, T., Vlemmix, T., and Van Roozendael, M.: Four years of ground-based MAX-DOAS observations of HONO and NO2 in the Beijing area, Atmos Chem Phys, 14, 765–781, https://doi.org/10.5194/acp-14-765-2014, 2014.

Irie, H., Takashima, H., Kanaya, Y., Boersma, K. F., Gast, L., Wittrock, F., Brunner, D., Zhou, Y., and Van Roozendael, M.: Eight-component retrievals from ground-based MAX-DOAS observations, Atmos Meas Tech, 4, 1027–1044, https://doi.org/10.5194/amt-4-1027-2011, 2011.

Kim, J., Jeong, U., Ahn, M. H., Kim, J. H., Park, R. J., Lee, H., Song, C. H., Choi, Y. S., Lee, K. H., Yoo, J. M., Jeong, M. J., Park, S. K., Lee, K. M., Song, C. K., Kim, S. W., Kim, Y. J., Kim, S. W., Kim, M., Go, S., Liu, X., Chance, K., Miller, C. C.,

https://doi.org/10.5194/egusphere-2024-589
Preprint. Discussion started: 15 March 2024

Al-Saadi, J., Veihelmann, B., Bhartia, P. K., Torres, O., Abad, G. G., Haffner, D. P., Ko, D. H., Lee, S. H., Woo, J. H., Chong, H., Park, S. S., Nicks, D., Choi, W. J., Moon, K. J., Cho, A., Yoon, J., Kim, S. kyun, Hong, H., Lee, K., Lee, H., Lee, S., Choi, M., Veefkind, P., Levelt, P. F., Edwards, D. P., Kang, M., Eo, M., Bak, J., Baek, K., Kwon, H. A., Yang, J., Park, J., Han, K. M., Kim, B. R., Shin, H. W., Choi, H., Lee, E., Chong, J., Cha, Y., Koo, J. H., Irie, H., Hayashida, S., Kasai, Y., Kanaya, Y., Liu, C., Lin, J., Crawford, J. H., Carmichael, G. R., Newchurch, M. J., Lefer, B. L., Herman, J. R., Swap, R. J., Lau, A. K. H., Kurosu, T. P., Jaross, G., Ahlers, B., Dobber, M., McElroy, C. T., and Choi, Y.: New era of air quality monitoring from space: Geostationary environment monitoring spectrometer (GEMS), Bull Am Meteorol Soc, 101, E1–E22, https://doi.org/10.1175/BAMS-D-18-0013.1, 2020.

Kleipool, Q.: OMI/Aura Surface Reflectance Climatology L3 Global Gridded 0.5 degree x 0.5 degree V3, 2010.

Kwon, H. A., Park, R. J., Abad, G. G., Chance, K., Kurosu, T. P., Kim, J., De Smedt, I., Van Roozendael, M., Peters, E., and Burrows, J.: Description of a formaldehyde retrieval algorithm for the Geostationary Environment Monitoring Spectrometer (GEMS), Atmos Meas Tech, 12, 3551–3571, https://doi.org/10.5194/amt-12-3551-2019, 2019.

Kwon, H. A., Park, R. J., Oak, Y. J., Nowlan, C. R., Janz, S. J., Kowalewski, M. G., Fried, A., Walega, J., Bates, K. H., Choi, J., Blake, D. R., Wisthaler, A., and Woo, J. H.: Top-down estimates of anthropogenic VOC emissions in South Korea using formaldehyde vertical column densities from aircraft during the KORUS-AQ campaign, Elementa, 9, https://doi.org/10.1525/elementa.2021.00109, 2021.

Lee, G. T., Park, R. J., Kwon, H.-A., Ha, E. S., Lee, S. D., Shin, S., Ahn, M.-H., Kang, M., Choi, Y.-S., Kim, G., Lee, D.-W., Kim, D.-R., Hong, H., Langerock, B., Vigouroux, C., Lerot, C., Hendrick, F., Pinardi, G., De Smedt, I., Roozendael, M. Van, Wang, P., Chong, H., Cho, Y., and Kim, J.: First evaluation of the GEMS formaldehyde retrieval algorithm against TROPOMI and ground-based column measurements during the in-orbit test period, EGUsphere [preprint], https://doi.org/10.5194/egusphere-2023-1918, 2023.

Lerot, C., Stavrakou, T., De Smedt, I., M̈uller, J. F., and Van Roozendael, M.: Glyoxal vertical columns from GOME-2 backscattered light measurements and comparisons with a global model, Atmos Chem Phys, 10, 12059–12072, https://doi.org/10.5194/acp-10-12059-2010, 2010.

Lerot, C., Hendrick, F., Van Roozendael, M., Alvarado, L. M. A., Richter, A., De Smedt, I., Theys, N., Vlietinck, J., Yu, H., Van Gent, J., Stavrakou, T., Müller, J. F., Valks, P., Loyola, D., Irie, H., Kumar, V., Wagner, T., Schreier, S. F., Sinha, V., Wang, T., Wang, P., and Retscher, C.: Glyoxal tropospheric column retrievals from TROPOMI -multi-satellite intercomparison and ground-based validation, Atmos Meas Tech, 14, 7775–7807, https://doi.org/10.5194/amt-14-7775-2021, 2021.

Li, J., Zhang, M., Tang, G., Wu, F., Alvarado, L. M. A., Vrekoussis, M., Richter, A., and Burrows, J. P.: Investigating missing sources of glyoxal over China using a regional air quality model (RAMS-CMAQ), J Environ Sci (China), 71, 108–118, https://doi.org/10.1016/j.jes.2018.04.021, 2018.

https://doi.org/10.5194/egusphere-2024-589
Preprint. Discussion started: 15 March 2024

Mason, J. D., Cone, M. T., and Fry, E. S.: Ultraviolet (250–550 nm) absorption spectrum of pure water, Appl Opt, 55, 7163, https://doi.org/10.1364/ao.55.007163, 2016.

Palmer, P. I., Jacob, D. J., Chance, K., Martin, R. V., Spurr, R. J. D., Kurosu, T. P., Bey, I., Yantosca, R., Fiore, A., and Li, Q.: Air mass factor formulation for spectroscopic measurements from satellites: Application to formaldehyde retrievals from the Global Ozone Monitoring Experiment, Journal of Geophysical Research Atmospheres, 106, 14539–14550, https://doi.org/10.1029/2000JD900772, 2001.

Serdyuchenko, A., Gorshelev, V., Weber, M., Chehade, W., and Burrows, J. P.: High spectral resolution ozone absorption cross-sections–Part 2: Temperature dependence, Atmos Meas Tech, 7, 625–636, 2014.

Silva, S. J., Heald, C. L., and Li, M.: Space-Based Constraints on Terrestrial Glyoxal Production, Journal of Geophysical Research: Atmospheres, 123, 13,583-13,594, https://doi.org/10.1029/2018JD029311, 2018.

Sinreich, R., Coburn, S., Dix, B., and Volkamer, R.: Ship-based detection of glyoxal over the remote tropical Pacific Ocean, Atmos Chem Phys, 10, 11359–11371, https://doi.org/10.5194/acp-10-11359-2010, 2010.

Spurr, R. J. D.: VLIDORT: A linearized pseudo-spherical vector discrete ordinate radiative transfer code for forward model and retrieval studies in multilayer multiple scattering media, J Quant Spectrosc Radiat Transf, 102, 316–342, https://doi.org/10.1016/j.jqsrt.2006.05.005, 2006.

Vandaele, A. C., Hermans, C., Simon, P. C., Carleer, M., Colin, R., Fally, S., Merienne, M.-F., Jenouvrier, A., and Coquart, B.: Measurements of the NO2 absorption cross-section from 42 000 cm− 1 to 10 000 cm− 1 (238–1000 nm) at 220 K and 294 K, J Quant Spectrosc Radiat Transf, 59, 171–184, 1998.

Volkamer, R., Spietz, P., Burrows, J., and Platt, U.: High-resolution absorption cross-section of glyoxal in the UV-vis and IR spectral ranges, J Photochem Photobiol A Chem, 172, 35–46, https://doi.org/10.1016/j.jphotochem.2004.11.011, 2005.

Volkamer, R., Barnes, I., Platt, U., Molina, L. T., and Molina, M. J.: Remote Sensing of Glyoxal by Differential Optical Absorption Spectroscopy (DOAS): Advancements in Simulation Chamber and Field Experiments, in: Environmental Simulation Chambers: Application to Atmospheric Chemical Processes. Nato Science Series: IV: Earth and Environmental Science, vol. 62, edited by: Barnes, I. and Rudzinski, K. J., Springer, Dordrecht, 2006.

Vrekoussis, M., Wittrock, F., Richter, A., and Burrows, J. P.: Atmospheric Chemistry and Physics Temporal and spatial variability of glyoxal as observed from space, Atmos. Chem. Phys, 4485–4504 pp., 2009.

Vrekoussis, M., Wittrock, F., Richter, A., and Burrows, J. P.: GOME-2 observations of oxygenated VOCs: What can we learn from the ratio glyoxal to formaldehyde on a global scale?, Atmos Chem Phys, 10, 10145–10160, https://doi.org/10.5194/acp-10-10145-2010, 2010.

Wang, Y. X., McElroy, M. B., Jacob, D. J., and Yantosca, R. M.: A nested grid formulation for chemical transport over Asia: Applications to CO, Journal of Geophysical Research D: Atmospheres, 109, 1–20, https://doi.org/10.1029/2004JD005237, 2004.

https://doi.org/10.5194/egusphere-2024-589
Preprint. Discussion started: 15 March 2024

Van Der Werf, G. R., Randerson, J. T., Giglio, L., Collatz, G. J., Mu, M., Kasibhatla, P. S., Morton, D. C., Defries, R. S., Jin, Y., and Van Leeuwen, T. T.: Global fire emissions and the contribution of deforestation, savanna, forest, agricultural, and peat fires (1997-2009), Atmos Chem Phys, 10, 11707–11735, https://doi.org/10.5194/acp-10-11707-2010, 2010.

Wittrock, F.: The retrieval of oxygenated volatile organic compounds by remote sensing techniques, PhD Thesis, 2006.

Wittrock, F., Richter, A., Oetjen, H., Burrows, J. P., Kanakidou, M., Myriokefalitakis, S., Volkamer, R., Beirle, S., Platt, U., and Wagner, T.: Simultaneous global observations of glyoxal and formaldehyde from space, Geophys Res Lett, 33, https://doi.org/10.1029/2006GL026310, 2006.

Woo, J. H.: KORUS emissions: A comprehensive Asian emissions information in support of the NASA/NIER KORUS-AQ mission, n.d.

https://doi.org/10.5194/egusphere-2024-589
Preprint. Discussion started: 15 March 2024

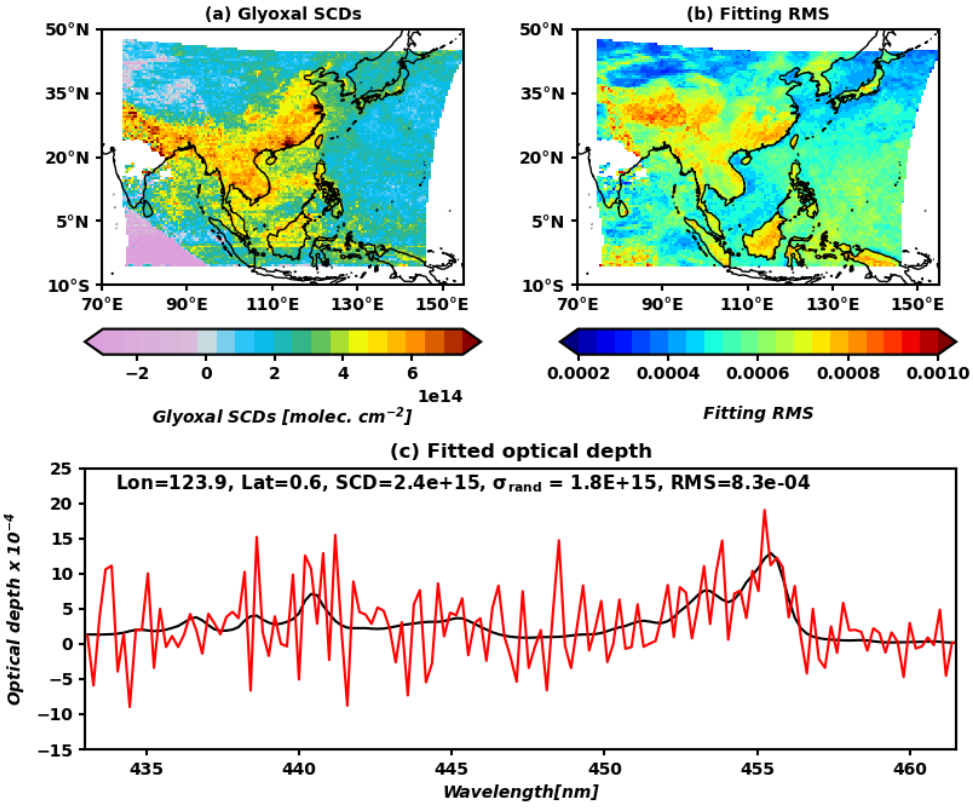

Figure 1. (a) GEMS glyoxal SCDs and (b) the root-mean-square values of the spectral fitting averaged for 02:45–06:45 UTC in August 2020. (c) Fitted optical depth (black line) and the sum of optical depth and fitting residual (red line).

https://doi.org/10.5194/egusphere-2024-589
Preprint. Discussion started: 15 March 2024

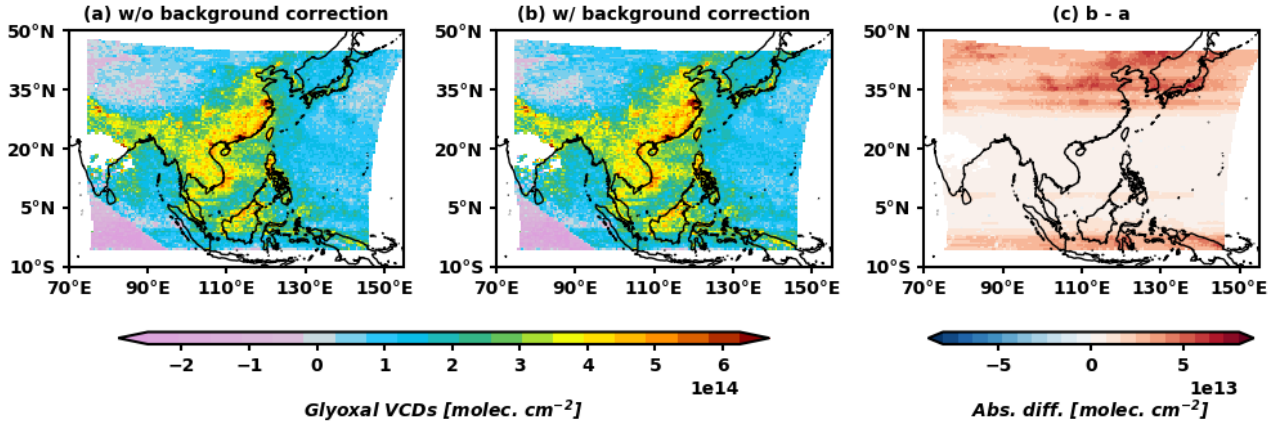

Figure 2. GEMS glyoxal VCDs retrieved (a) without background correction and (b) with background correction for 02:45–06:45 UTC in August 2020. (c) The absolute difference between (a) and (b).

https://doi.org/10.5194/egusphere-2024-589
Preprint. Discussion started: 15 March 2024

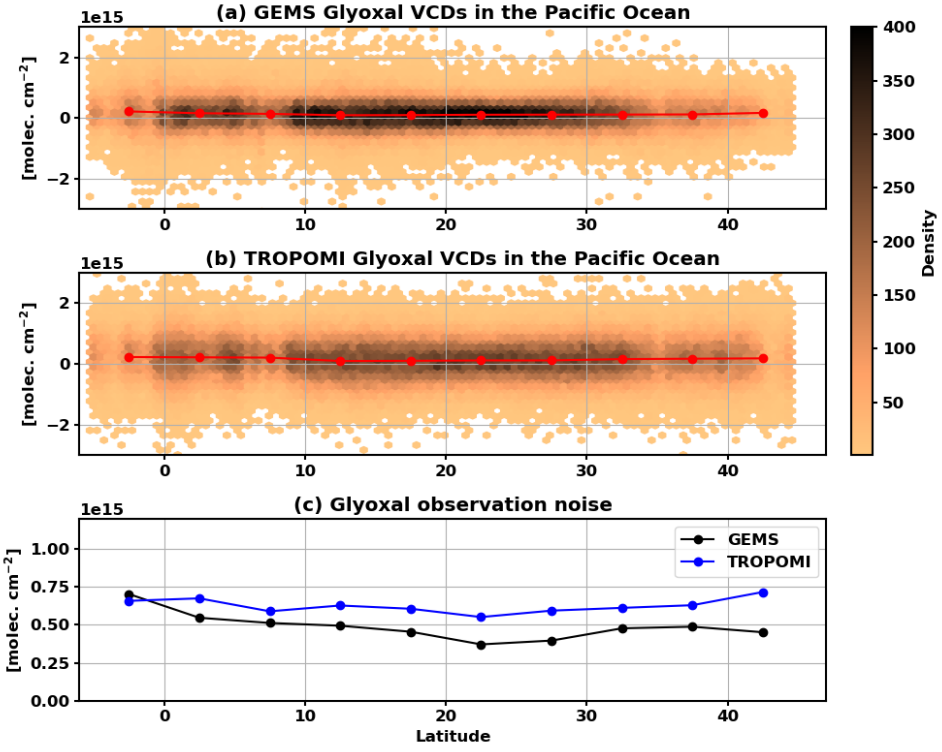

Figure 3. (a) GEMS and (b) TROPOMI glyoxal VCDs in the ocean over 130–146° E on 3 August 2020. We filtered out pixels over land with cloud cover (cloud fraction > 0.4). The hexagons filled with colormap indicate the density of all data, and the red line indicate the data binned in 5° latitude bands. (c) The standard deviation of the binned data for GEMS and TROPOMI.

https://doi.org/10.5194/egusphere-2024-589
Preprint. Discussion started: 15 March 2024

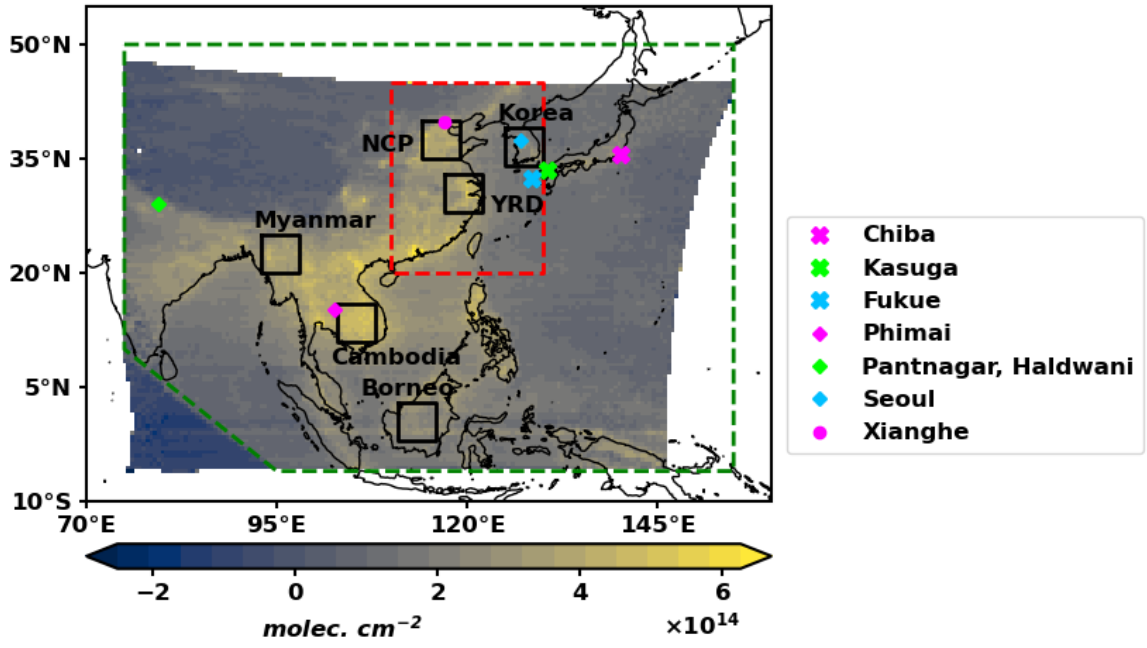

Figure 4. The green dashed line indicates the area defined as Domain 1, and the red dashed line indicates the area defined as Domain 2 (20–45° N, 110–130° E) in Figure 5. The black boxes indicate areas where glyoxal VCDs are averaged in Figure 6. Markers indicate the locations of the MAX-DOAS stations in Figure 8 and Figure 9. The colormap in the background represents GEMS glyoxal VCDs averaged from August 2020 to July 2021 at 00:45–07:15 UTC.

https://doi.org/10.5194/egusphere-2024-589
Preprint. Discussion started: 15 March 2024

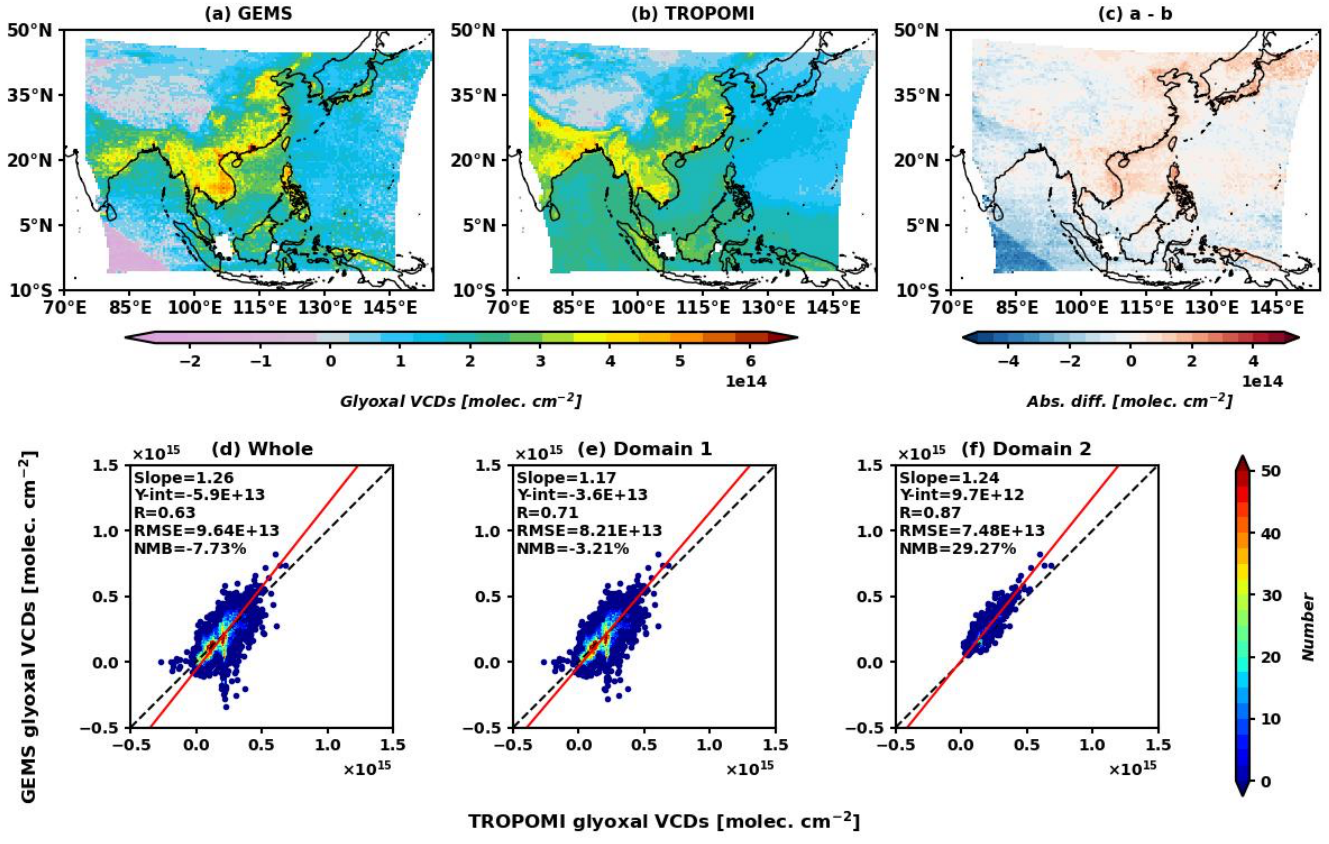

Figure 5. (a) GEMS and (b) TROPOMI glyoxal VCDs averaged from August 2020 to July 2021 at 11:30–15:30 local time. (c) The absolute difference between GEMS and TROPOMI glyoxal VCDs. Scatter plots comparing GEMS and TROPOMI glyoxal VCDs for the (d) whole domain, (e) Domain 1, and (f) Domain 2 indicated in Figure 4.

470

https://doi.org/10.5194/egusphere-2024-589
Preprint. Discussion started: 15 March 2024

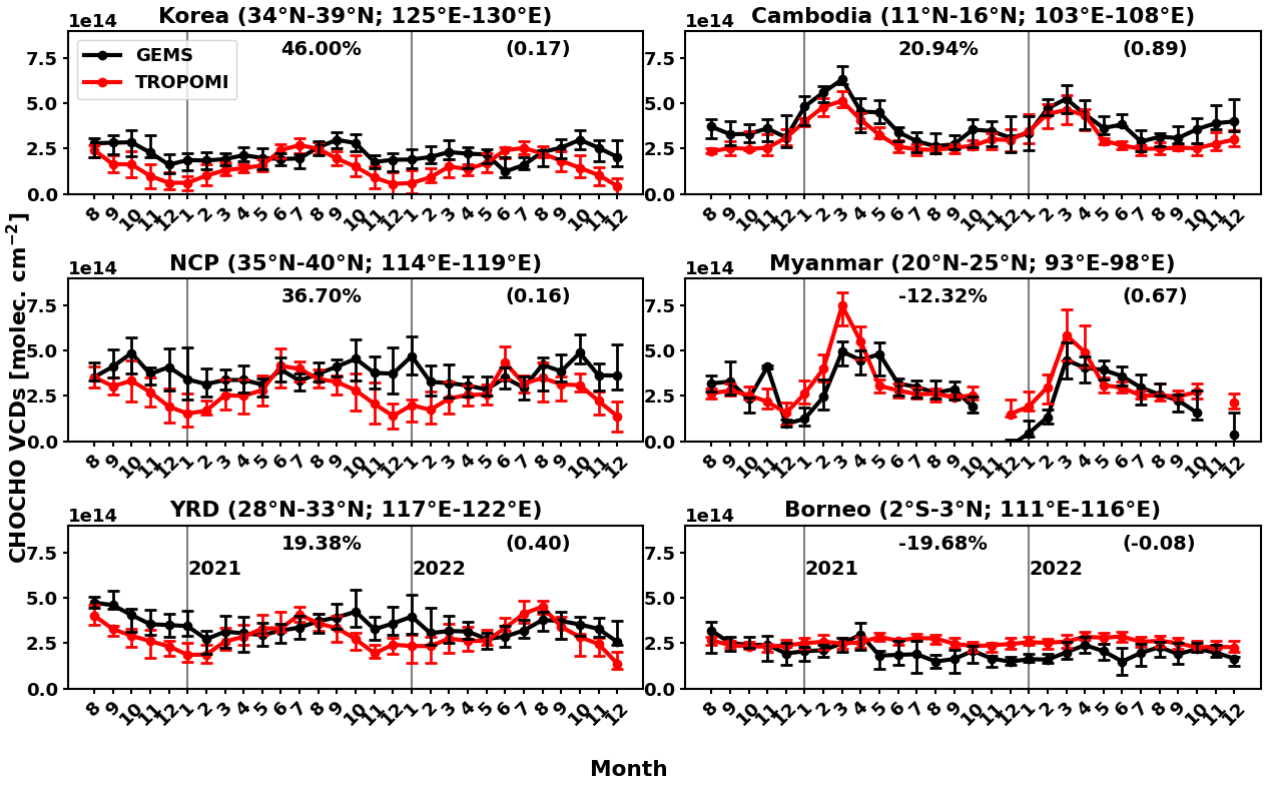

Figure 6. Monthly mean glyoxal VCDs from GEMS (black line) and TROPOMI (red line) from August 2020 to December 2022 at 11:30–15:30 local time. The error bars indicate the 25th and 75th percentiles of daily VCDs averaged for each domain depicted in Figure 4. The numbers on the left denote the normalized mean bias of GEMS VCDs with respect to TROPOMI VCDs, and the numbers in the parentheses denote the correlation coefficient of GEMS and TROPOMI VCDs.

https://doi.org/10.5194/egusphere-2024-589
Preprint. Discussion started: 15 March 2024

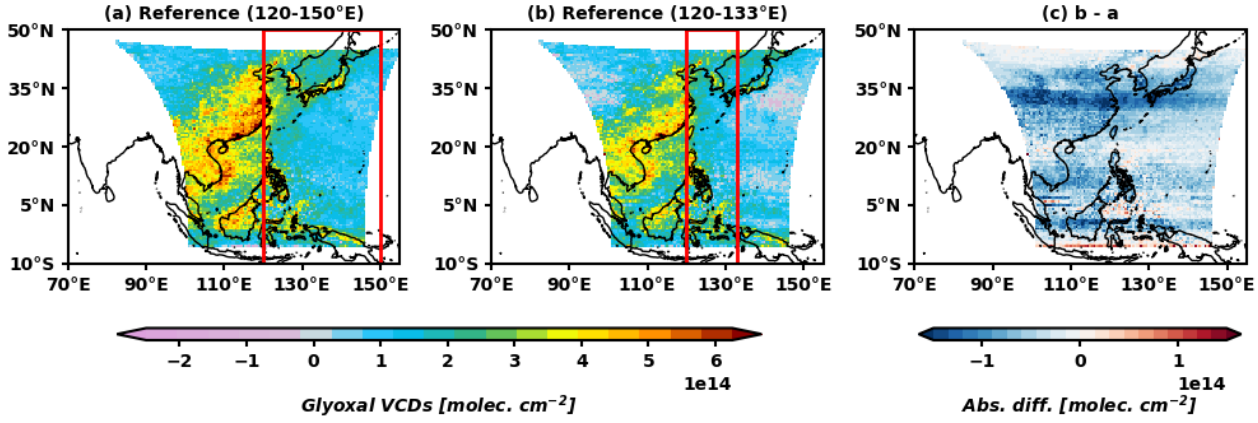

Figure 7. GEMS glyoxal VCDs averaged for the observations taken as nominal daily scan for 02:45–06:45 UTC in August 2020. Panel A shows the VCDs retrieved with the reference sector of 120–133° E, and panel B shows those of 120–150° E. The red boxes in panel a and b indicates reference sector used to retrieve each glyoxal VCDs. (c) The absolute difference between panel a and b.

485

https://doi.org/10.5194/egusphere-2024-589
Preprint. Discussion started: 15 March 2024

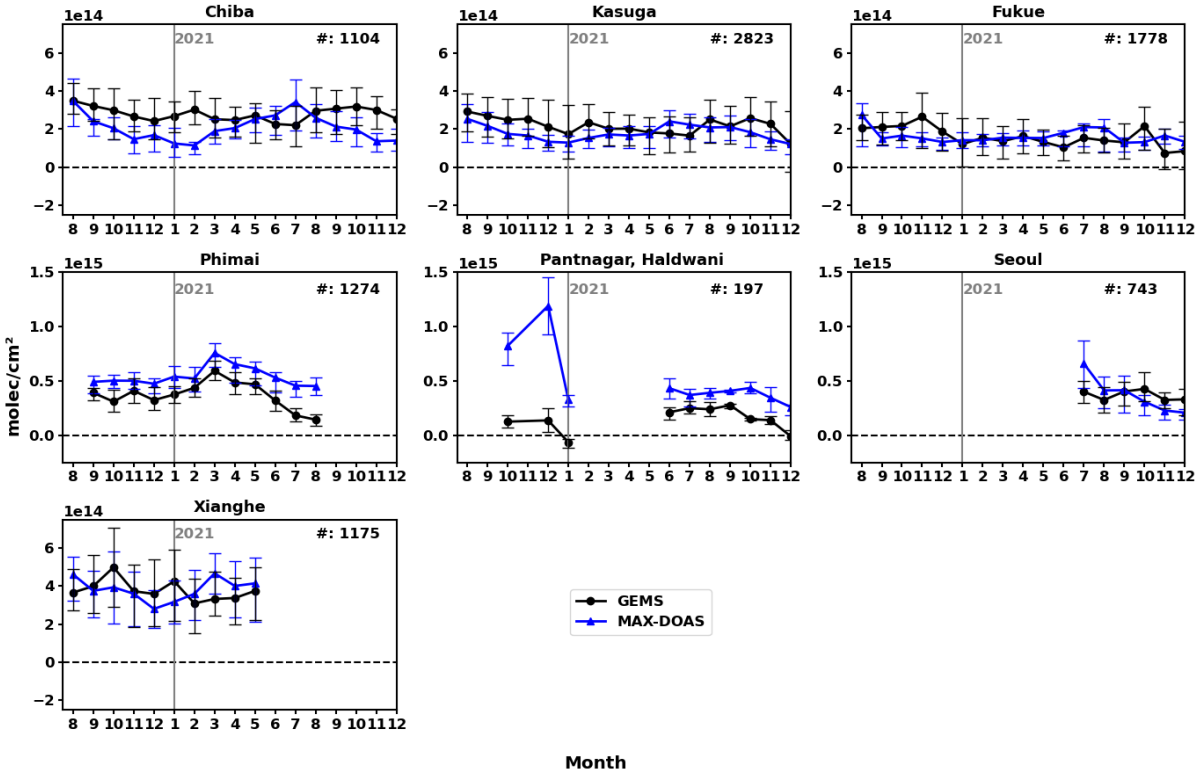

Figure 8. Monthly mean glyoxal VCDs from GEMS (black line) and MAX-DOAS (blue line) from August 2020 to December 2021. The error bars indicate the 25th and 75th percentiles of hourly averaged VCDs. The numbers on the right denote the number of hourly data co-located at each station.

https://doi.org/10.5194/egusphere-2024-589
Preprint. Discussion started: 15 March 2024

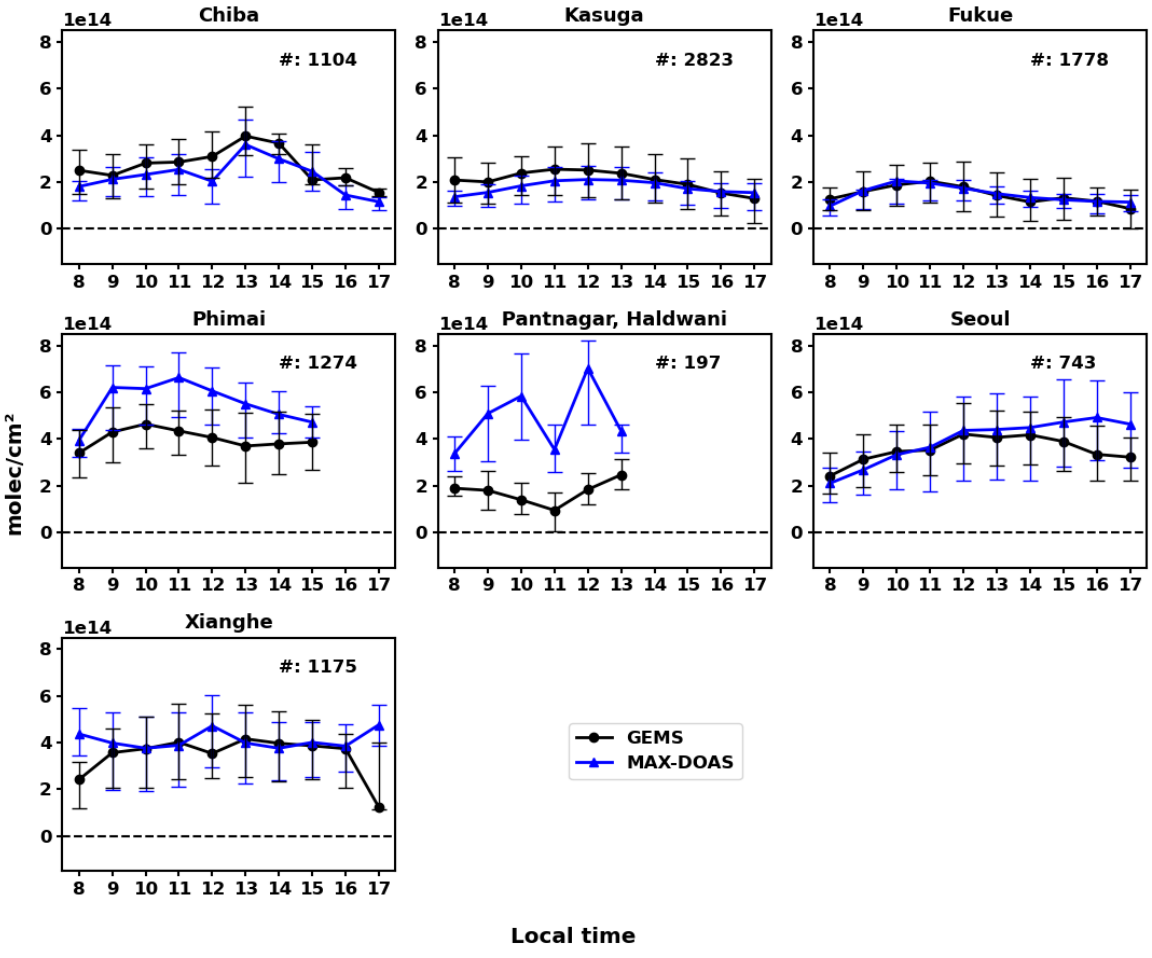

Figure 9. Hourly mean glyoxal VCDs from GEMS (black line) and MAX-DOAS (blue line) from August 2020 to December 2021. The error bars indicate the 25th and 75th percentiles of hourly averaged VCDs. The numbers on the right denote the number of hourly data co-located at each station.